Experiments in Fluids, Volume 49, Number 3, 2010, Pages 683-699

Hypersonic interference heating in the vicinity of surface protuberances

Estruch-Samper, D.; MacManus, D.G.; Stollery, J.L.; Lawson, N.J.; Garry, K.P.

Department of Aerospace Sciences, Cranfield University, Cranfield, Bedfordshire, MK43 0AL, UK

Abstract

The understanding of the behaviour of the flow around surface protuberances in hypersonic vehicles is developed and an engineering approach to predict the location and magnitude of the highest heat transfer rates in their vicinity is presented. To this end, an experimental investigation was performed in a hypersonic facility at freestream Mach numbers of 8.2 and 12.3 and Reynolds numbers ranging from $Re_\infty/m=3.35\times10^6$ to $Re_\infty/m=9.35\times10^6$. The effects of protuberance geometry, boundary layer state, freestream Reynolds number and freestream Mach number were assessed based on thin-film heat transfer measurements. Further understanding of the flowfield was obtained through oil-dot visualizations and high-speed schlieren videos. The local interference interaction was shown to be strongly three-dimensional and to be dominated by the incipient separation angle induced by the protuberance. In interactions in which the incoming boundary layer remains unseparated upstream of the protuberance the highest heating occurs adjacent to the device. In interactions in which the incoming boundary layer is fully separated ahead of the protuberance the highest heating generally occurs on the surface just upstream of it except for low-deflection protuberances under low-Reynolds freestream flow conditions in which case the heat flux to the side is greater.

Notation

α	protuberance deflection angle, degrees
α_R	coefficient of resistivity, K^{-1}
δ	boundary layer thickness with edge at $U = 0.99U_\infty$, m
μ	dynamic viscosity, $kg\cdot m^{-1}\cdot s^{-1}$
θ	temperature relative to wall, $= T_{aw} - T_w$
$\varnothing$	diameter, m
ρ	density, $kg\cdot m^{-3}$
$\left(\sqrt{\rho c_p k}\right)_g$	thermal property of gauges, $J\cdot K^{-1}\cdot m^{-2}\cdot s^{-0.5}$
c_p	specific heat capacity at constant pressure, $J\cdot kg^{-1}\cdot K^{-1}$
G	system gain, =2.06 at 0.1kHz – 5kHz signal frequency
h	protuberance height, m
k	thermal conductivity, $W\cdot m^{-1}\cdot K^{-1}$
l	characteristic linear dimension, m
L	separation length ahead of protuberance-plate junction, m
M	Mach number
Nu	Nusselt number, $= St\,\mathrm{Re}\,\mathrm{Pr}$
p	static pressure, Pa
P_D	drive pressure, Pa
Pr	Prandtl number, assumed =1
q	heat flux, $= \left(\sqrt{\rho c_p k}\right)_g \overline{V_2} \Big/ \left(\alpha_R V_1 G\right)$, $W\cdot m^{-2}$
r	recovery factor, assumed =1
Re	Reynolds number, $= \rho U l / \mu$
Re/m	Reynolds number per unit length, $= \rho U / \mu$
Re_L	Reynolds number based on L, $= \rho_\infty U_\infty L / \mu_\infty$
$Re_{x,k}$	Reynolds number based on x_k, $= \rho_\infty U_\infty x_k / \mu_\infty$
$Re_{y,cl}$	Reynolds number based on y_{cl}, $= \rho_\infty U_\infty y_{cl} / \mu_\infty$
St	Stanton number, $= q / \left[\rho_\infty U_\infty c_p \theta\right]$
t	time, s
T	static temperature, K
U	axial velocity, $m\cdot s^{-1}$

V_1	initial voltage across gauge, V
$\overline{V_2}$	average output voltage of integrated signal across effective run duration, $V \cdot s^{-0.5}$
W	protuberance width, m
x	longitudinal distance, m
y	lateral distance from centreline, m
z	normal distance from flat plate, m

Subscripts

∞	freestream conditions
$*$	reference value
aw	adiabatic wall
cl	relative to centreline
e	conditions at boundary layer edge
h	based on protuberance height
i	incipient conditions
k	relative to protuberance leading edge
le	relative to flat plate leading edge
o	total or stagnation conditions
s	shock wave
u	undisturbed conditions at protuberance location
w	conditions on the wall
x	based on local values

1. Introduction

Surface protuberances are frequently unavoidable in the design of hypersonic vehicles in the form of control surfaces but also as smaller elements of the order of the boundary layer thickness such as junction screws or bolts, hinges, instrumentation and cable protection pads, stiffeners, control modules and motors, etc. (Guoliang and Guiqing 2004; Davis 2008; Wang et al. 2009). In any of these forms, the protuberance interferes with the freestream flow and results in a three-dimensional interaction which induces high local aerodynamic heating. Whereas the protuberances can be made of advanced heat-resistant materials it is the heating of the vehicle surface which is generally of the highest concern in practical engineering applications (Stollery et al. 2008).

Most experimental studies on surface protuberances in hypersonic laminar flow focused on their effectiveness as boundary layer trips rather than on the induced heat flux increase – e.g. Sterret et al. (1967) and Stainback (1969) who studied spheres, cylinders and triangular and spherical rod trips. Other studies also investigated sinusoidal surfaces – e.g. Bertram and Wiggs (1963); Arrington (1968) and Weinstein (1970). On the other hand, most studies on turbulent flows have been on fin protuberances - e.g. Jones (1964), Price and Stallings (1967), Coleman and Lemmon (1973), Neumann and Hayes (1981) and Wang et al. (1998). The most relevant experimental studies on surface protuberances to date are those performed by Hung and Clauss (1980) and Hung and Patel (1984), who studied the fully separated interaction induced by cylindrical and rectangular protuberances under both laminar and turbulent conditions. Based on their work, distinction can be made between tall ($h>2Ø$ or $h>2W$), short ($h<Ø$ or $h<W$) and wide protuberances ($Ø \rightarrow \infty$ or $W \rightarrow \infty$, i.e. quasi-two-dimensional). Their main results showed that the highest heat transfer in the vicinity of tall protuberances is independent of their height whereas around short and wide protuberances this is independent of the width but strongly dependent on the protuberance height.

Overall, previous experimental studies have shown that the local interaction induced by the presence of a protuberance in hypersonic flow depends mainly on its geometry (height, width, etc.) and on the freestream flow conditions (incoming boundary layer, Reynolds number, Mach number, etc.). Nevertheless, most studies to date have considered tall protuberances in the form of control surfaces and a generic predictive approach is not available due to the lack of experimental data encompassing all the main parameters involved (Nestler 1985). To this end, using a hypersonic gun tunnel, the present investigation presents an experimental dataset of heat flux measurements in the vicinity of surface protuberances from a Mach 8.2 and 12.3 flow. In particular, 3-dimensional short compression ramp protuberances with finite span and of the order of the boundary layer thickness are considered. High-resolution quantitative measurements were taken with thin-film gauges and further flow characteristics were identified using oil-dot visualizations and a high-speed schlieren system.

2. Experimental study

Experimental work was performed in the Cranfield University Hypersonic Gun Tunnel at freestream Reynolds numbers ranging from $Re_\infty/m=3.35x10^6$ to $Re_\infty/m=9.35x10^6$ and at freestream Mach numbers of $M_\infty=8.2$ and $M_\infty=12.3$. Further details on this facility can be found in Needham (1963).

2.1 Flow establishment and operating conditions

The duration of the effective hypersonic flow stream varied depending on the nozzle and on the operating conditions, which were changed by using different driver pressures as shown in Table 1. The initial barrel pressure was atmospheric for all the tests. At Mach 12.3, the drive pressure was restricted to $13.8x10^6$ Pa (2000 psig) since lower freestream conditions could result in low temperatures which could lead to air liquefaction and damage to the facility and instrumentation. The initial wall temperature was T_w=295±5 K. The rapid establishment of the flow (1-2 ms) - even in cases involving strong separation regions - was assessed from the high-speed schlieren results during all the tests.

M_∞	P_D [MPa]	$P_{0,\infty}$ [MPa]	$T_{0,\infty}$ [K]	ρ_∞ [kg·m^{-3}]	U_∞ [m·s^{-1}]	Re_∞ / m [m^{-1}]	t_{run} [ms]
8.2±0.05	13.8 ± 1%	10.9 ± 1%	1290 ± 3%	0.0371 ± 7.1%	1553 ± 1.6%	$9.35x10^6$ ± 7.6%	31±0.5
8.2±0.05	10.3 ± 1%	8.2 ± 1%	1180 ± 3%	0.0304 ± 7.1%	1486 ± 1.6%	$8.06x10^6$ ± 7.7%	39±0.5
8.2±0.05	6.9 ± 1%	5.4 ± 1%	1040 ± 3%	0.0230 ± 7.1%	1395 ± 1.6%	$6.57x10^6$ ± 7.7%	52±0.5
12.3±0.05	13.8 ± 1%	10.9 ± 1%	1290 ± 3%	0.0054 ± 6.2%	1584 ± 1.5%	$3.35x10^6$ ± 7.5%	176±0.5

Table 1 Experimental test conditions.

2.2 Case study

To simulate surface protuberances on a hypersonic vehicle, a 150mmx265mm flat plate was used to replicate the surface of the vehicle and protuberance models were fixed on it as shown in Fig. 1. The protuberances were three-dimensional compression corners with a finite span and height (Table 2). During some of the tests, transition was forced using a strip of 1mm-high 30° triangular vortex generators (VGs) with a 3.5mm spanwise spacing which were placed 20mm downstream of the flat plate leading edge in order to trip the natural laminar boundary layer. This configuration was selected as the most suitable one for the present application given that it was expected to provide fully turbulent conditions without spanwise non-uniformities at the location of the protuberance ($x_{le} \approx$ 175mm) as shown in previous studies by Vannahme (1994) and Prince (1995). The spanwise 2-dimensionality of the turbulent boundary layer was demonstrated in their liquid crystal flow visualizations and heat flux measurements, which showed vortex breakdown to occur between 100mm and 140mm from the plate leading edge. The use of side fences was therefore considered unnecessary as subsequently corroborated by the whole dataset of heat flux measurements obtained in the present investigation which in all cases shows a uniform undisturbed heat flux value in the regions outside of the interaction. A further assessment on VG effectiveness and on the 2-dimensionality of the flow upstream of the protuberance can be found in Estruch (2009a). At the location of the protuberance ($x_{le} \approx$ 175mm), the turbulent boundary layer thickness was estimated from the schlieren images to be δ_u=5.0mm ±0.5mm at Mach 8.2 and δ_u=6.0mm ±0.5mm at Mach 12.3. The laminar boundary layer obtained without vortex generators at Mach 8.2 and at that same location had a thickness of approximately δ_u=2.5mm ±0.25mm also based on analysis of the schlieren images. Sufficient margin was allowed in order to avoid interference of the flat plate leading edge Mach cones with the interaction induced by the protuberance.

The investigation was centred on the datum case of a $\alpha = 30°$ protuberance at a freestream Mach number of $M_\infty=8.2$, Reynolds number of $Re_\infty/m=9.35x10^6$ in a turbulent flow as shown in Table 2. A protuberance twice the height and another one twice the width with respect to the datum configuration were considered to assess the effects of protuberance dimensions. The effect of protuberance deflection angle was studied with similar models but with deflection angles of $\alpha = 15°$, 45°, 60° and 90° and the case of a surface protuberance with forward deflection was also considered ($\alpha = 135°$). The effect of boundary layer state, Reynolds number and Mach number on the magnitude of the highest heat transfer was assessed for almost the full range of deflection angles ($\alpha = 15°$ to $\alpha = 135°$). The only exception was the $\alpha = 15°$ protuberance which was not considered in the study of Reynolds number effect due to the limited information this configuration was expected to provide.

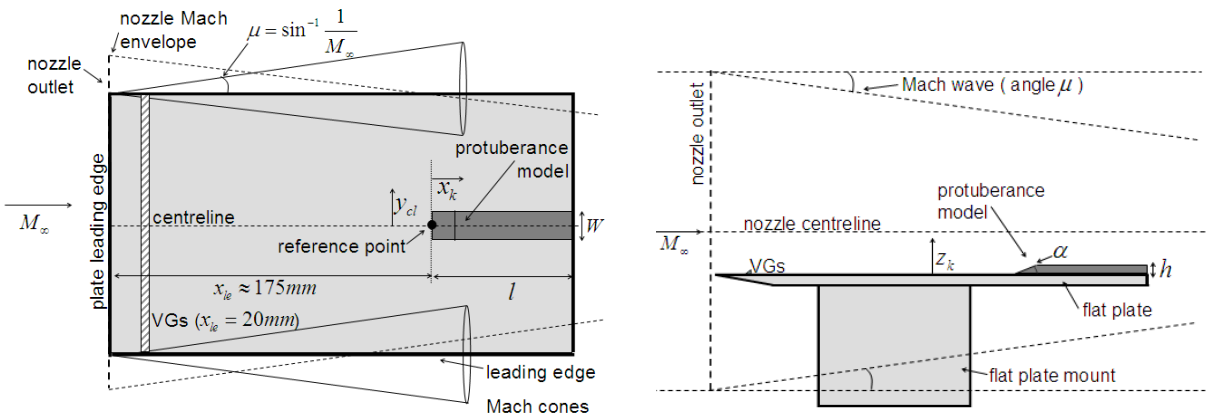

(a) (b)

Fig. 1 Test model arrangement: plan view (a) and side view (b).

Study	M_∞	Re_∞ / m [m^{-1}]	α [°]	h [mm]	W [mm]	VGs
datum	8.2	9.35x10^6	30	5.0	13.5	Yes
h/δ_u effect	8.2	9.35x10^6	30	10.0	13.5	Yes
W/δ_u effect	8.2	9.35x10^6	30	5.0	27.0	Yes
α effect	8.2	9.35x10^6	15,45,60,90	5.0	13.5	Yes
forward α effect	8.2	9.35x10^6	135	5.0	13.5	Yes
b. l. state effect	8.2	9.35x10^6	15,30,45, 60,90,135	5.0	13.5	No
Re_∞ effect	8.2	8.06x10^6	30,45,60,90,135	5.0	13.5	Yes
	8.2	6.57x10^6	30,45,60,90,135	5.0	13.5	Yes
M_∞ effect	12.3	3.35x10^6	15,30,45, 60,90,135	5.0	13.5	Yes

Table 2 Summary of present study.

2.3 Heat flux measurements

Optical methods are usually preferred to obtain non-intrusive measurements in high-speed wind tunnel testing but their application to measure surface heating in hypersonic flows is particularly restricted by a number of factors as reviewed by Estruch et al (2009b). Consequently, eight thin-film gauges were used in the present study with the purpose of obtaining high-resolution high-accuracy measurements of the flux of heat to the surface surrounding the protuberance models. The sensor elements were approximately 1.2mm-long and 0.3mm-wide and were very fragile (Olivier 2009). To avoid changing the gauges from one location to another between the different runs, they were fixed as an 8-off thin-film module which only needed to be changed to a second location on the plate. A corresponding blank module was made and placed in the redundant plate cavity during each test case. The position of the model on the flat plate was also changed so that its relative distance to the gauges would allow a final distributed pattern of measurement points around the protuberance. Measurements were performed with a maximum spatial resolution of 2mm in the longitudinal (x) and lateral directions (y) in the cases required. Special care was taken in the selection of the measurement points so that enough resolution would be obtained in the vicinity of the model to capture the hot spot. The thin film elements were also oriented perpendicular to the direction of the highest heat flux gradients (which take place normal to the front and side of the model) to improve discretisation of the hot spot. The determination of heat transfer (refer to notations) was based on the analogy between the flow of heat into a semi-infinite material and the flow of current into an R-C circuit as described in more detail in the work of Schultz and Jones (1973).

2.4 Measurement error and accuracy

In order to assess the accuracy of the system, stagnation heat flux measurements were performed at the nose of a hemisphere with a radius of 5.0mm, at freestream conditions of M_∞=8.2 and Re_∞/m=9.35x10^6. The stagnation heat flux relation from Fay and Riddell (1958) was used to obtain an estimate of the heat transfer at that point. A measure of the repeatability of the measurements was performed based on three independent tests. An average stagnation heat flux value of 130.9 W/cm^2 (St_o = 22.7x10^{-3}) was determined

and measurements differed up to ±1.3% from the average. This was at the same time 1.3% lower relative to the analytical prediction ($q_o = 132.6$ W/cm^2, $St_o = 23.0\text{x}10^{-3}$) thus giving an indication of the expected accuracy of the system for this type of flow.

A further uncertainty analysis was performed by considering a typical transducer error of 5% in the calibration of the thermal property of each individual gauge $\left(\sqrt{\rho c_p k}\right)_g$ and of 2% in the calibration of the thermal coefficient of resistivity α_R as quoted by the manufacturer. The error related to the input voltage of the gauges V_1 (1%), the measurement resolution of the output voltage $\overline{V_2}$ (0.03%) and the calibration of the system gain G (1.6%) was also accounted for together with the uncertainties related to the freestream flow conditions (Table 1) and wall temperature (1.7%). With a random error of 3.5% at 99.6% confidence and a maximum systematic error of 9.5% based on the uncertainties mentioned, a total combined uncertainty of ±10% in the measurement of Stanton number was estimated, which is similar to the error range achieved in other similar experimental studies as reviewed by Simmons (1995). Stanton number is used throughout the present study to provide a non-dimensional measure of heat flux with respect to the potential heating rate of the local flow. The conservative total uncertainty of ±10% - which is significantly higher than the error found in the accuracy assessment - is consistently considered.

2.5 Flat plate measurements

Heat flux measurements from the undisturbed flat plate boundary layer were taken at different freestream gun tunnel conditions. The state of the boundary layer was inferred from the schlieren images along with a comparison between measured heat transfer and the corresponding analytical estimates. The appearance of the boundary layer in the schlieren images distinguished between fully laminar conditions and transitional/turbulent conditions. This was qualitatively observed by sampling lines of pixel data at several stations from the markedly higher intensity of the laminar boundary layer in comparison to this of a transitional or turbulent boundary layer as shown in Section 3. In cases where there was a doubt on whether the boundary layer was fully turbulent or transitional, comparison was made between the heat transfer measurements and the corresponding predicted estimates using Eckert's reference temperature method (Eckert 1956; White 2006). Underpredictions about 20%-30% were expected in the turbulent estimations (Meador and Smart 2005). In this way, in the cases where heating was closer to the laminar estimation - despite not appearing as a laminar boundary layer in the schlieren image - a transitional boundary layer was effectively identified. Based on this evidence the inferred state of the boundary layer is presented in Table 3.

	Experiments		Estimates		Boundary layer state		
	No VG q (W/cm^2)	With VG q (W/cm^2)	Lam. q (W/cm^2)	Turb. q (W/cm^2)	Lam.	Tran.	Turb.
M_∞=8.2, Re_∞/m=9.35x10^6	1.8	5.9	1.7	5.6	X	---	X
M_∞=8.2, Re_∞/m=8.06x10^6	---	3.8	1.3	3.9	---	---	X
M_∞=8.2, Re_∞/m=6.57x10^6	---	1.0	0.9	2.3	---	X	---
M_∞=12.3, Re_∞/m=3.35x10^6	---	0.9	0.4	0.7	---	---	X

Table 3 Experimental measurement of heat flux from undisturbed boundary layer at location of protuberance (x_{le}≈175mm) and assessment of boundary layer state considering 30% underprediction.

3. Protuberance interference heating

Results of the experimental investigation on the local interaction induced by surface protuberances are presented in this section. The distances in the plots are non-dimensionalised with respect to the freestream Reynolds number and where appropriate they are presented in the original dimensions in the experiments. Although this is not common practice, the non-dimensionalisation of distance based on other parameters more commonly used (e.g. W, h, δ_u, etc.) is considered misleading in this case since it does not provide a suitable scaling in all the interactions according to the present results. Instead, the freestream Reynolds number (Section 3.6) appears to scale with the dimensions of the flow features linked with the increased heating in these interactions (Section 4.5). It must therefore be kept in mind that the respective Reynolds numbers in the text effectively correspond to non-dimensional distances (refer to notations).

3.1 Datum case

The experimental investigation was centred around the datum configuration of a 30°-deflected protuberance at Mach 8.2 and with a unit Reynolds number of $Re_\infty/m=9.35\times10^6$. A turbulent boundary layer with thickness δ_u=5.0mm ± 0.5mm was obtained with the vortex generator strip. The h/δ_u ratio of the protuberance was thus equal to 1 and W/δ_u was 2.7. In this configuration, the boundary layer just ahead of the protuberance is primarily undisturbed until it impacts on the model. An attached shock is observed in the schlieren image (Fig. 2). The larger shock spanning from left to right in the image is the weak shock which originates at the flat plate leading edge.

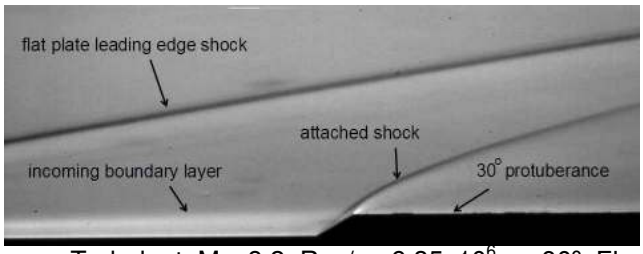

Fig. 2 Schlieren image. Turbulent, M_∞=8.2, $Re_\infty/m=9.35\times10^6$, α=30º. Flow from left to right.

Heat flux measurements in the vicinity of this protuberance are shown in Fig. 3 using the local Stanton number. The oil flow visualizations showed almost no upstream influence of the protuberance but highlighted regions of higher skin friction to the side. Consequently, the highest heating is also measured in this region to the side of the protuberance. A local maximum of $St_{\max}$=2.9x10^{-3} ($q_{\max}$=17.0W/cm^2) is measured at $\mathrm{Re}_{x,k}=9.8\times10^4$ (x_k =10.5mm) and $\mathrm{Re}_{y,cl}=7.5\times10^4$ (y_{cl} =8mm) while ahead of the model heating rates are slightly lower than the undisturbed value of St_u=1.0x10^{-3} (q_u =5.9 W/cm^2). The latter values can be explained due to the slight thickening of the boundary layer at that location which results in lower temperature gradients through it. It could also be speculated that the heat flux reduction ahead of the protuberance could be induced by Görtler vortices; however, no evidence of these phenomena has been found in the present study.

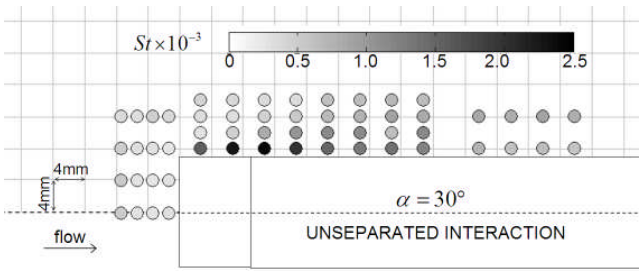

Fig. 3 Heat flux in the vicinity of datum protuberance: plan view. Turbulent, M_∞=8.2, $Re_\infty/m=9.35\times10^6$.

3.2 Effect of protuberance dimensions

The effect of protuberance width and protuberance height was briefly studied. Due to the small working section and high-resolution requirements to which the test models were subject, a brief assessment was performed considering the cases where the W/δ_u ratio was doubled relative to the datum and another where h/δ_u was similarly doubled. The wind tunnel conditions during these tests were the same as those considered in the datum case. Two interactions with an unseparated boundary layer ahead of the protuberance were observed in the schlieren images which were qualitatively similar to the datum case in Fig. 2.

Heat flux measurements along the centreline ahead of the h/δ_u=1 and h/δ_u=2 protuberances match within 98.7% of the peak value as shown in Fig. 4a. The behaviour of the boundary layer is therefore insensitive to the height of the protuberance. Measurements to the side of the models show that the effects of height and width on the hot spot are also negligible in practical terms ($St_{\max}$ =2.5x10^{-3} to 2.9x10^{-3} are measured in the three cases, Fig. 4b). These findings suggest that the maximum heating in the vicinity of surface protuberances is independent of protuberance height when the boundary layer ahead of the protuberance remains unseparated. This is in contrast to equivalent studies by Hung and Clauss (1980) and Hung and Patel (1984) in which the boundary layer was fully separated ahead of the protuberance. The present investigation, however, has not considered h/δ_u ratios lower than 1. It is possible that the height of the protuberance has an effect on the heat flux augmentation in such cases, particularly if the protuberance is totally submerged into the subsonic portion of the boundary layer. Nevertheless, it is unlikely that the heat

flux augmentation is higher than with taller protuberances and thus they are not considered of particular importance. The effect of width within short span protuberance configurations (about $W/\delta_u \leq 10$) on the magnitude of the hot spot is negligible in interactions with an upstream unseparated boundary layer as in short and wide protuberances with upstream boundary layer separation (Hung and Patel, 1984).

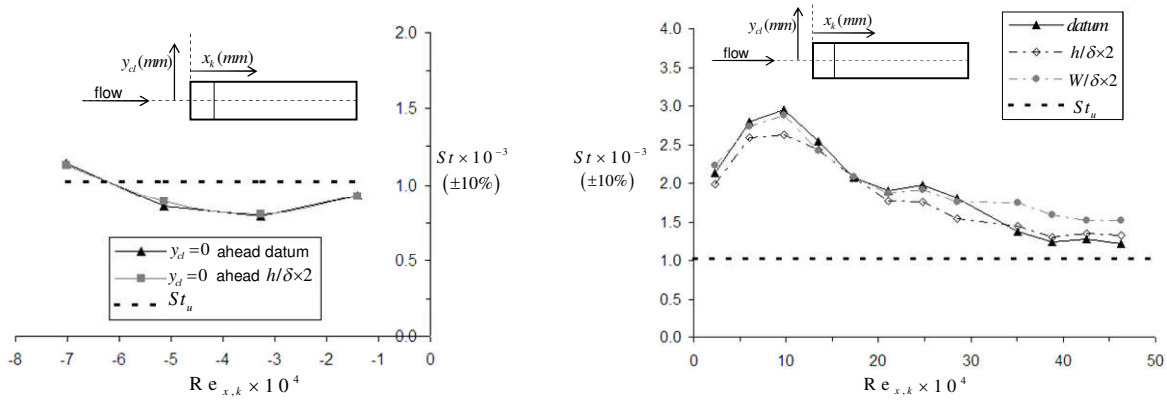

(a) (b)

Fig. 4 Heat flux ahead of datum ($h/\delta_u=1$) and $h/\delta_u=2$ configurations, α=30º (a) and adjacent to datum, h/δ_ux2 and W/δ_ux2 cases, y_{cl}=8mm (b).

3.3 Effect of protuberance deflection angle

Protuberance models with the same height, width and length as the datum protuberance, but with leading edge angles of α=15°, α=45°, α=60° and α=90°, were used to assess the effect of protuberance deflection angle (Table 2). The freestream conditions were the same as for the datum study (M_∞=8.2, $Re_\infty/m=9.35\times10^6$, turbulent). Instantaneous schlieren images for each of the leading edge deflection angle configurations are shown in Figs. 5a-5d. As the deflection angle increases and thus the local interaction becomes stronger a separation region is observed ahead of the protuberance. At these freestream conditions, the boundary layer remains unseparated upstream of the model with the α=15° protuberance (Fig. 5a) and the datum case (α=30°, Fig. 2) and it is fully separated for α=45°, α=60° and α=90° (Figs. 5b-5d). This is in good agreement with previous experimental studies on two-dimensional compression ramp interactions which report incipient separation angles of approximately α_i=25°-35° at hypersonic speeds (Elfstrom 1971) as further discussed in Section 4.2.

High-speed schlieren images were recorded at frame rates of up to 50 kHz and show that the upstream flow is unsteady when the local interference interaction induces the separation of the boundary layer ahead of the protuberance. In these cases there is a clear oscillation of the boundary layer separation shock. For interactions in which the upstream boundary layer remains unseparated, the flow appears to be steady throughout the effective run duration. The location of the shock was captured through a digital image processing method as described in Estruch et al. (2008) (Fig. 6). No clear frequency could be determined due to the predominantly broadband nature of the shock oscillation. Recent investigations on similar interactions seem to indicate that this is mainly due to the separation mechanism of the boundary layer (Estruch et al. 2009c, 2009d).

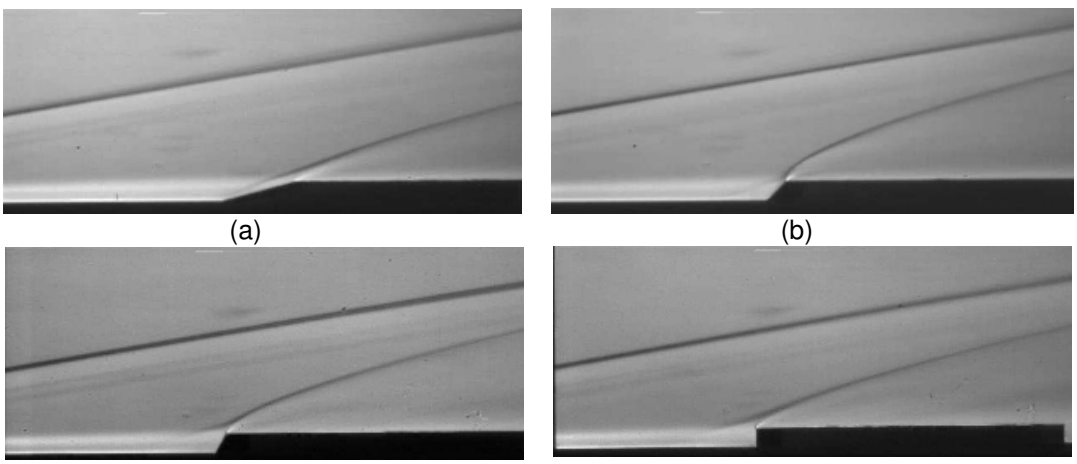

(a) (b)

(c) (d)

Fig. 5 Schlieren images. Turbulent, M_∞=8.2, $Re_\infty/m=9.35\times10^6$, α=15° (a), α=45° (b), α=60° (c) and α=90° (d). Flow from left to right.

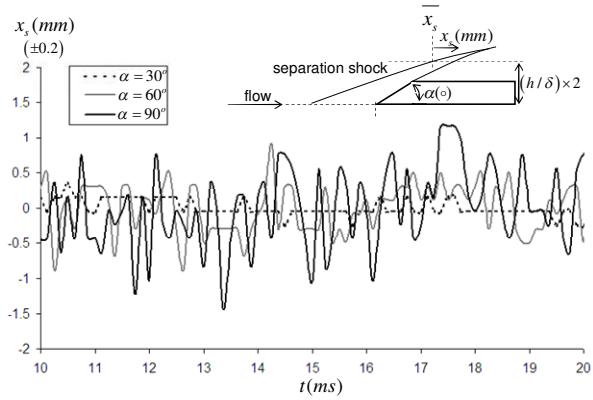

Fig. 6 Shock wave oscillation between t=10ms and t=20ms from the start of the run. M_∞=8.2, Re_∞/m=9.35x10^6, turbulent.

The heat flux ahead of the protuberances in which the upstream boundary layer is unseparated (α=15° and α=30°) remains almost undisturbed while in the cases in which an upstream flow separation is induced (α=45° to α=90°) the heat flux in the separation region increases and reaches its highest value just ahead of the protuberance (Figs. 7 and 8). A direct relationship between protuberance deflection angle and the magnitude and extent of the heat flux augmentation ahead of the protuberance is thus observed in the latter cases. As expected from previous experiments (see e.g. Kuehn 1959; Holden 1964) the extent of the separation region increases with deflection angle due to the higher adverse pressure gradient imposed to the incoming boundary layer. It is thus shown that the local interference interaction is strongly dependent on whether the boundary layer ahead of the protuberance remains unseparated or whether it is fully separated. The following classification is followed to distinguish between two types of interference interactions:

-Unseparated interactions: Those in which the incoming boundary layer remains unseparated upstream of the protuberance (α=15° and α=30° in this case) – although not to the side. In such interactions, an increase in heat flux occurs to the side of the protuberance whereas heat flux rates of the same order or indeed lower than the corresponding undisturbed value take place ahead of it.

-Fully separated interactions: Those in which the incoming boundary layer is fully separated ahead of the protuberance (α=45°, α=60° and α=90°). In this case, the highest heating rates are found just ahead of the protuberance where a separation bubble occurs. Increased heating is also found to the side of the protuberances and with a similar magnitude to that measured in unseparated interactions. In weak separated interactions (α=45°) the highest heating is found both ahead of the protuberance and to its side and therefore a clear hot spot cannot be so clearly identified.

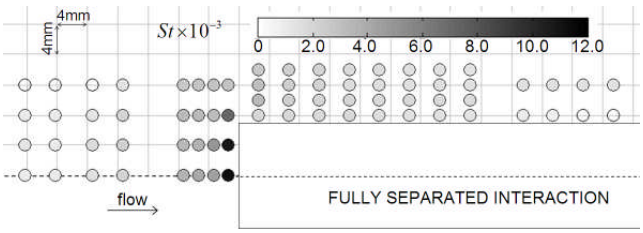

Fig. 7 Heat flux in the vicinity of α=90° protuberance: plan view. Turbulent, M_∞=8.2, Re_∞/m=9.35x10^6.

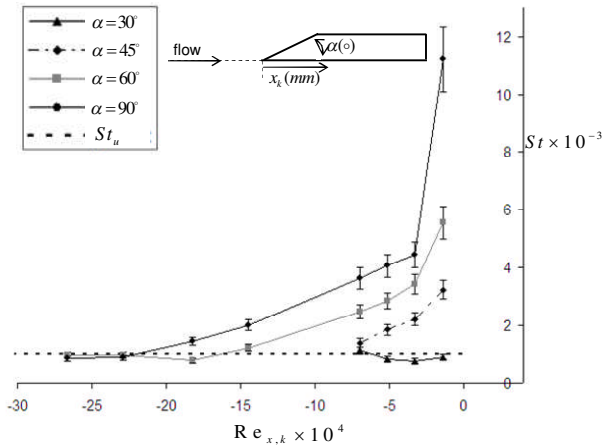

Fig. 8 Heat flux along the centreline (y_{cl}=0mm) as a function of protuberance deflection angle. Turbulent, M_∞=8.2, Re_∞/m=9.35x10^6, α=30º to α=90º.

3.4 Effect of forward deflection

A protuberance with an effective forward deflection angle of α=135° was considered. A schlieren image of this configuration is shown in Fig. 9, where a larger separation region ahead of the model is seen with respect to the lower angle cases. Comparing this with the measurements ahead of the α=90° model, Fig. 10 shows that the heat flux increases progressively as the flow separates ahead of the protuberance and therefore the region of intensified heating is larger in this case due to the larger separated flow region. The highest heat flux occurs just ahead of the protuberance and with values of 41.2% higher than with the α=90º configuration in this case although high heating is also found to the side with a value of $St_{\max,side}$=2.6x10^{-3}. As shown in more detail in Section 3.6 it is believed that the hot spot was not captured in this configuration and an actual increase in about 106.4% with respect to the α=90º case is expected.

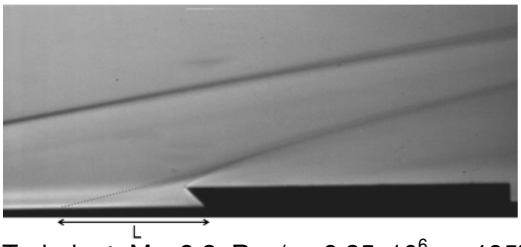

Fig. 9 Schlieren image. Turbulent, M∞=8.2, Re∞/m=9.35x10^6, α=135º. Flow from left to right.

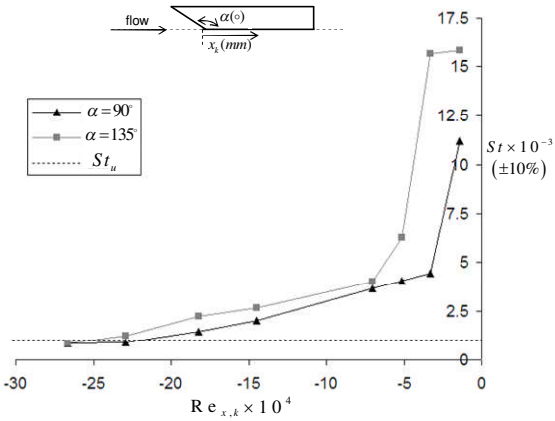

Fig. 10 Heat flux ahead of α=135º and α=90º cases. Turbulent, M∞=8.2, Re∞/m=9.35x10^6, y_{cl}=0mm.

3.5 Effect of boundary layer state

To assess the influence of the incoming boundary layer on the heat flux distributions, experiments were performed at the same freestream conditions used in the datum study but without the vortex generators on the flat plate. This allowed a laminar boundary layer to develop. The boundary layer thickness at the location of the protuberance was δ_u = 2.5mm ± 0.25mm. Schlieren images for the laminar cases ranging from angles α=15° to α=135° are shown in Figs. 11a-f. The boundary layer separates ahead of the protuberance in all the cases. Recall that for the datum case (turbulent, α=30°) the boundary layer remains attached ahead of the protuberance (Fig. 2). This is due to the increased sensitivity of laminar boundary layers to adverse pressure gradients which result in lower incipient separation angles. At these test conditions this is estimated to be α_i<15° (Chapman et al. 1958; Hakkinen et al. 1959; Sterrett and Emery 1960). As also expected from these two-dimensional ramp studies, the length of the separation region for the laminar boundary layer cases is larger than in the turbulent configurations (Figs. 2, 5 and 9) and increases with protuberance deflection angle in a similar way. The extent of the upstream separated region for laminar conditions is around 3 times longer than under turbulent conditions for each corresponding angle. Consequently, with the same protuberance geometry and operating conditions, the effect of the incoming boundary layer has a strong impact on the local heat flux augmentation.

The magnitude of the heat flux to the side of the α=30° protuberance is shown in Fig. 12a comparing the laminar and turbulent cases at axial locations corresponding to $\mathrm{Re}_{x,k} = 21.0\times10^4$ (x_k=22.5mm, laminar) and $\mathrm{Re}_{x,k} = 9.8\times10^4$ (x_k=10.5mm, turbulent) where the maximum side heating was measured for each case. The maximum side heat flux for turbulent conditions in terms of Stanton number is about 15% higher than under laminar conditions. Measurements to the side of the α=15° and α=30° protuberances under laminar

conditions are shown in Fig. 12b, where the maximum side heat flux appears to be unaffected by deflection angle. For practical purposes, an approximate value of the maximum heating adjacent to the protuberance can therefore be obtained by considering the heat flux to the side to be independent of boundary layer state, protuberance dimensions and deflection angle.

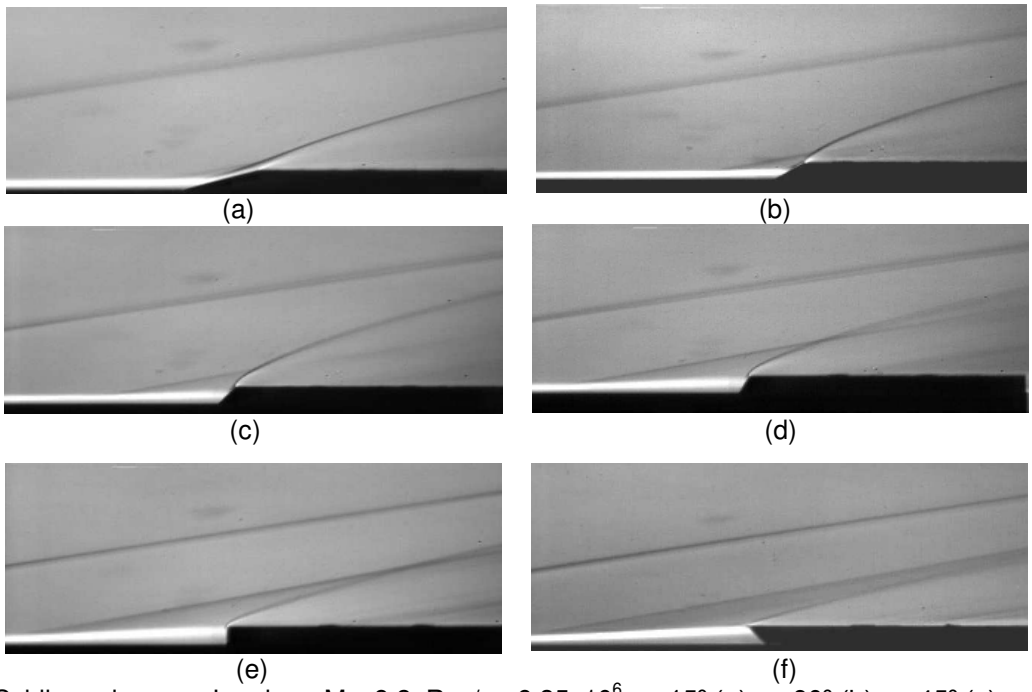

Fig. 11 Schlieren images. Laminar, M_∞=8.2, Re_∞/m=9.35x10^6, α=15º (a), α=30º (b), α=45º (c), α=60º (d), α=90º (e) and α=135º (f).

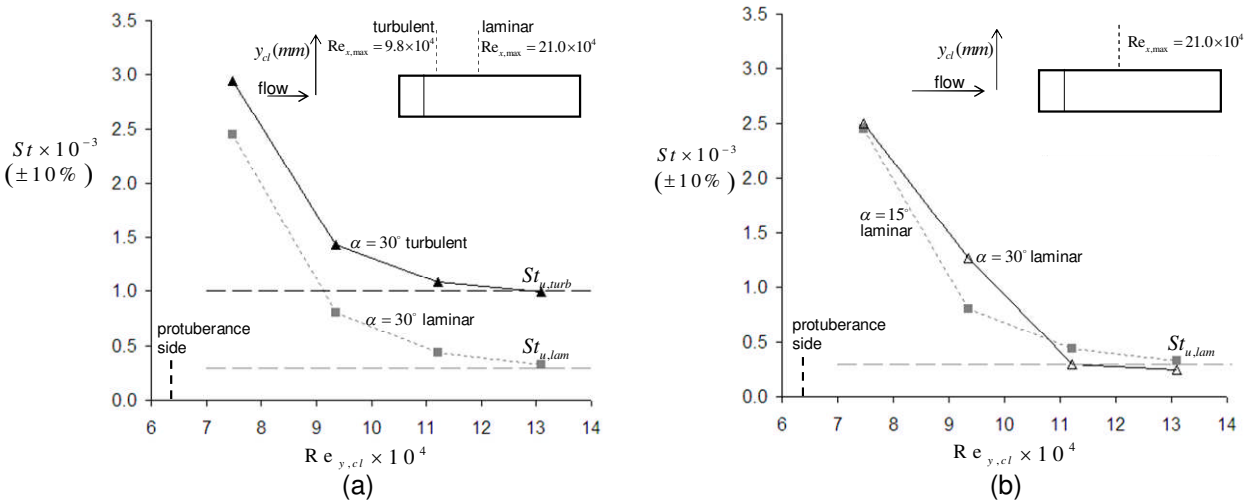

Fig. 12 Spanwise distribution of heat transfer and peak axial locations to the side of α=30º protuberance for laminar and turbulent conditions (a) and to the side of α=15º and α=30º models for laminar conditions (b).

As expected based on the experiments of Hung and Patel (1984) in laminar flow higher heating rates than the undisturbed heat flux are measured ahead of the protuberance in fully separated interactions. At the low deflection angles, the heat flux amplification is small. A comparison between the magnitude of the hot spots for different deflection angles and boundary layer state is shown in Fig. 13a. The peak heating is found just ahead of the protuberances ($\mathrm{Re}_{x,k} = -1.4\times10^4$, x_k=-1.5mm) except for the forward deflection model (α=135°). In this case, whereas under turbulent conditions it is located at $\mathrm{Re}_{x,k} = -1.4\times10^4$ (x_k=-1.5mm), in laminar flow this is found slightly further upstream at $\mathrm{Re}_{x,k} = -3.3\times10^4$ (x_k=-3.5mm) (Fig. 13b). For the range of angles from α=15° to α=90° the peak heat transfer magnitude is almost the same at both laminar and turbulent conditions and regardless of h/δ_u ratio with a difference of 0.5% for the α=90° interaction. Only the α=135° protuberance departs from the trend where it reaches a value of St_u=23.1x10^{-3} (q_u=132.7 W/cm^2) for a laminar boundary layer in comparison to St_u=19.1x10^{-3} (q_u=97.4 W/cm^2) for the turbulent

case. The independence on the state of the incoming boundary layer state is most likely because the incoming laminar boundary layer becomes transitional or even fully turbulent through the interaction as suggested by the present measurements, which is believed to be directly linked to the 3-dimensionality of the interactions. This statement is supported by the analysis of results at all the test conditions and is further demonstrated in Section 4. The difference for the forward deflection case is attributed to the lack of measurement resolution ahead of the α=135° protuberance where a slightly more complex interaction takes place as suggested by Fig. 13, where the expected heat flux trend based on these assumptions is indicated. This is further supported by the interpretation of the flow field based on the present experimental results and related numerical simulations (Section 4.5). The highest heating in the M_∞=8.2, Re_∞/m=9.35x10^{6,} turbulent case is expected to occur at a location between ($\mathrm{Re}_{x,k} = -3.3\times10^4$) x_k=-3.5mm and $\mathrm{Re}_{x,k} = -1.4\times10^4$ (x_k=-1.5mm).

In general, based on this limited range of data, these results suggest that the maximum heat transfer rate is not strongly dependent on the state and thickness of the boundary layer for both unseparated and fully separated interactions. Although a more intensive investigation would be required to separate the effect of boundary layer thickness and boundary layer state, the consistent similitude in magnitude between the hot spot in these cases (≈0.5%) despite the very different boundary layer thickness (δ_u is 100% higher in the turbulent case than in the laminar one) provides supporting evidence to this statement. Although the boundary layer state does not have a large influence on the magnitude of the hot spot, it does have a strong effect on the extent of the local interaction and thus on the region where heating rates are increased relative to the corresponding undisturbed value. It is worth noting that the highest heating rates in these cases are of the same order as the corresponding stagnation point heating by considering the protuberance height to be equal to an effective hemisphere radius $h = R_N = 5mm$ (Section 2.4). This approximate analogy shows that extremely high heating rates can be present in the vicinity of surface protuberances.

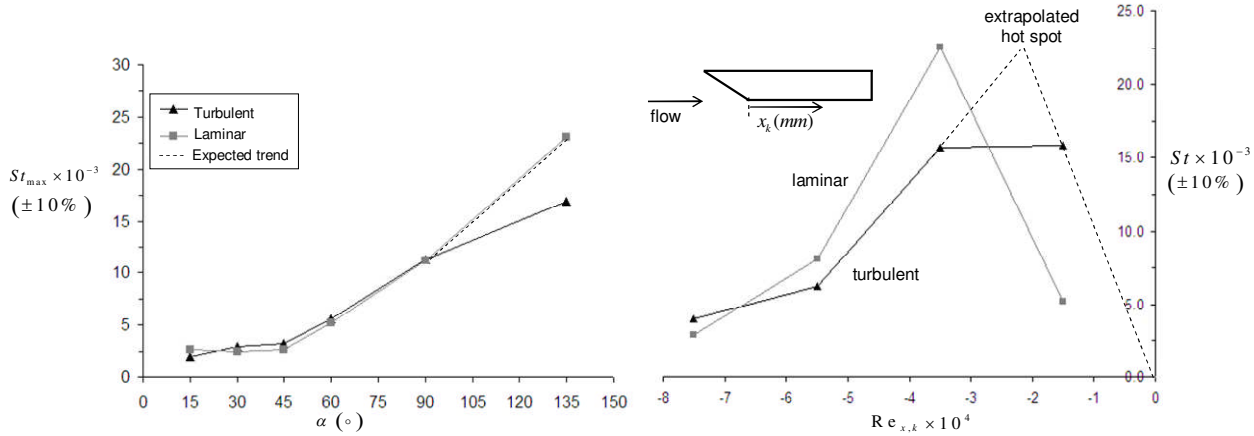

(a) (b)

Fig. 13 Peak heat flux as a function of deflection angle under laminar and turbulent conditions. M_∞=8.2, Re_∞/m=9.35x10^6, α=15° to α=135° (a) and ahead α=135° protuberance at laminar and turbulent conditions. M_∞=8.2, Re_∞/m=9.35x10^6 (b).

3.6 Effect of Reynolds number

The effect of freestream Reynolds number was studied by changing the drive pressure of the wind tunnel at Mach 8.2 conditions. Measurements were performed at a driver pressure of 13.8x10^{6}Pa (Re_∞/m=9.35x10^6), 10.3x10^{6}Pa (Re_∞/m=8.06x10^6) and 6.9x10^{6}Pa (Re_∞/m=6.57x10^6). The extent of the separation region ahead of fully separated interactions based on the high-speed schlieren images is presented in the next section. Separated interactions with a fully turbulent incoming boundary layer at Re_∞/m=8.06x10^6 are slightly larger than those at Re_∞/m=9.35x10^6 and with a fully turbulent boundary layer as well. As described by Needham and Stollery (1966a, 1966b) for two-dimensional ramp interactions, the length of the separated region is expected to increase with Reynolds numbers in fully laminar and fully turbulent flows but the opposite trend is expected in transitional flows. Although the latter trend is observed in the present case, there is a high level of confidence in the inferred state of the boundary layer as shown in Section 2.5 – i.e. fully laminar or fully turbulent at Re_∞/m=9.35x10^6 and Re_∞/m=8.06x10^6 conditions - and also based on the incipient angle α_i as mentioned in Sections 3.3 and 3.5. The observed trend is attributed to the 3-dimensionality of the present interactions which results in a re-energising process of the flow through the interaction similar to this occurring in transitional flow (Needham and Stollery, 1966a, 1966b) and thus in a higher resistance to separation of the boundary layer at higher Reynolds numbers.

Similarly to the $Re_\infty/m=9.35x10^6$ tests, an unseparated interaction is also obtained at $Re_\infty/m=8.06x10^6$ and at a deflection angle of α=30°, and fully separated interactions are obtained at the higher angles. At $Re_\infty/m=6.57x10^6$ the boundary layer is transitional and therefore a direct comparison cannot be made. Similar to the laminar case, the α=30° protuberance is fully separated at $Re_\infty/m=6.57x10^6$ and much larger separation areas are observed in this case due to the transitional nature of the boundary layer. A comparison of the maximum heat flux values for the different Reynolds number cases is shown in Fig. 14. As before, the peak heat flux is found to the side of the protuberance in the unseparated interactions and ahead of the protuberance in the fully separated interactions. The forward deflection angle (α=135º) is the only case which slightly deviates from this general trend. Also, the peak heating is weakly sensitive to Reynolds number. Although the location of the hot spot to the side of the protuberances in unseparated interactions is not so clear as in fully separated interactions where sharp gradients are present, a clear trend is noticed which shows that the reattachment of the flow to the side of the protuberance takes place at farther distances from the protuberance leading edge at lower Reynolds numbers. This is explained through the reduced ability of the boundary layer to reattach at low Reynolds numbers and the expectation that the highest heat flux rates at this location are caused by the flow reattachment (Section 4.6). The Reynolds number is therefore suitable to non-dimensionalise the separation length L and other distances characteristic of these interactions.

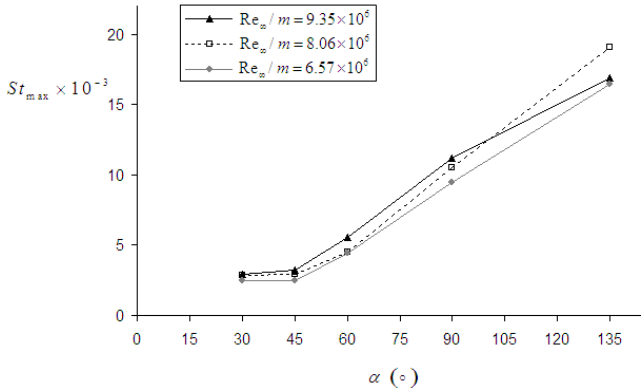

Figs. 14 Peak heat flux for different deflection angles (α=30º to α=135º) and freestream Reynolds numbers ($Re_\infty/m=6.57x10^6$, $8.06x10^6$ and $9.35x10^6$) at $M_\infty=8.2$.

3.7 Effect of Mach number

Tests were performed at a freestream Mach number of 12.3 using vortex generators which provided a fully turbulent boundary layer with thickness δ_u=6.0mm ± 0.5mm. Due to the complexity involved in the operation of the facility and the complete experimental rig, and also to the costs, the investigation was limited by the number of runs and thus tests at Mach 12.3 laminar conditions were considered of secondary importance given that the hot spot magnitude was expected to be independent of the incoming boundary layer state as shown by the Mach 8.2 measurements (Section 3.5), which suggest that the incoming boundary layer becomes transitional or even fully turbulent through the interaction. It is nevertheless acknowledged that further data would have provided more consistency to this statement.

At Mach 12.3 turbulent conditions, based on the schlieren images, the length of the separation region ahead of the protuberance is smaller than in the laminar and transitional boundary layer cases ($Re_\infty/m=6.57x10^6$ with VGs and $Re_\infty/m=9.35x10^6$ without VGs) but significantly longer than in the turbulent cases at $M_\infty=8.2$ ($Re_\infty/m=8.06x10^6$ and $Re_\infty/m=9.35x10^6$ with VGs). Figure 15 shows the extent of the separation length (L) ahead of the model (i.e. distance from boundary layer separation shock to plate-protuberance junction) in non-dimensional form for all the test cases. An uncertainty of ±10% is assumed based on the unsteadiness of some of the interactions and on the extrapolation of the separation shock wave to the flat plate. Presented in this form, the separation region at $M_\infty=12.3$ is smaller than in the turbulent cases at the lower Mach number of $M_\infty=8.2$. This was expected since the resistance of boundary layers to separation increases significantly with Mach number (Kuehn 1959).

Heat flux measurements for the α=30° model are presented in Fig. 16. Based on the schlieren results this is an unseparated interaction. The heat flux ahead is slightly lower than the undisturbed heat flux as in the corresponding Mach 8.2 turbulent case (Fig. 3). High heating rates are observed adjacent to the protuberance with the highest heat transfer rate taking place far downstream from the leading edge ($Re_{x,k}=35.1\times10^4$, x_k=37.5mm) given that the boundary layer reattaches farther at low Reynolds numbers. The highest heating to the model's side is found at $Re_{y,cl}=3.4\times10^4$ (y_{cl}=10mm) in this case, which is farther from the model side than in the previous cases ($Re_{y,cl}=2.7\times10^4$, y_{cl}=8mm). This is also attributed to the low Reynolds number which results in larger side recirculations (Section 4.5).

As in the other conditions, the maximum heating rates increase with deflection angle. Ahead of the α=135° case, the highest heat flux measurements are found a little further upstream of it ($\mathrm{Re}_{x,k} = -3.3\times10^4$, x_k=-3.5mm) which is also observed in the transitional M_∞=8.2, $Re_\infty/m=6.57\times10^6$ and in the laminar M_∞=8.2, $Re_\infty/m=9.35\times10^6$ cases. At high Reynolds number conditions the highest heating is found just ahead of the model ($\mathrm{Re}_{x,k} = -1.4\times10^4$, x_k=-1.5mm). Consequently, in fully separated interactions the measurements can be classified in two groups: those where the boundary layer is more robust and thus the separation region ahead of the protuberance and the distance from the leading edge to the side hot spot are shorter, and those with weaker boundary layers, longer separation regions and side hot spots farther from the protuberance leading edge as further discussed in Section 4.

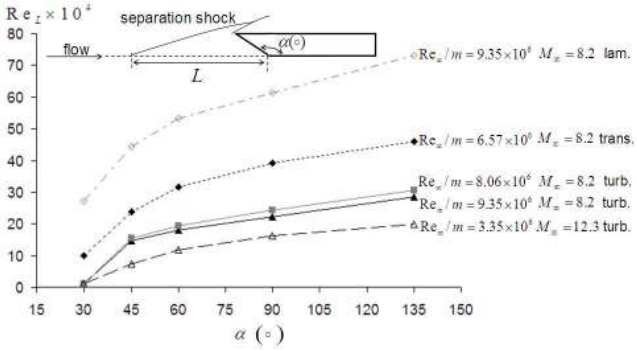

Fig. 15 Non-dimensional separation length ahead of protuberances at all the conditions considered.

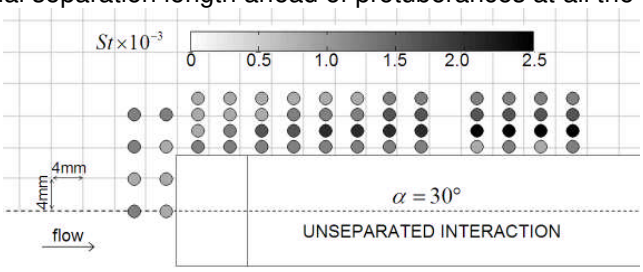

Fig. 16 Heat flux in the vicinity of α=30º protuberance. Turbulent, M_∞=12.3, $Re_\infty/m=3.35\times10^6$.

4. Hot spot estimation approach

Based on the current experimental results, a method is developed to predict the location and magnitude of the peak heat flux in the vicinity of a surface protuberance on a hypersonic vehicle.

4.1 Hot spot location and magnitude

The magnitude of the hot spots for all configurations is summarized in Fig. 17. The magnitude of the maximum heat flux generally increases with both deflection angle and Reynolds number. The measurements at Mach 8.2 group closer together and the Mach 12.3 measurements are much lower (about half the Mach 8.2 value), for which a clear effect of Mach number is also shown. The maximum heat flux in the unseparated interactions is practically the same for all the conditions simulated. These results provide further evidence that a consistent set of data has been acquired and that the measurement spatial resolution has been sufficient to capture the principal effects. As identified previously, the exception to this is the turbulent case with M_∞=8.2, $Re_\infty/m=9.35\times10^6$, α=135º.

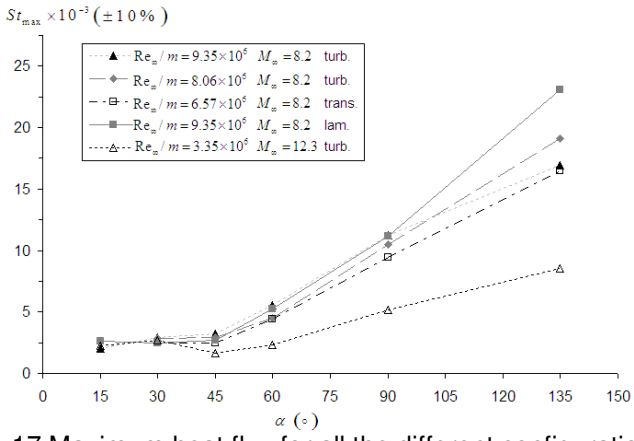

Fig. 17 Maximum heat flux for all the different configurations.

4.2 Incipient separation conditions

In order to predict the location and magnitude of the hot spot around a protuberance it is thus vital to evaluate whether the local interference interaction is unseparated or fully separated. An incipient protuberance deflection angle (α_i) needs to be estimated based on the state of the incoming boundary layer (laminar, transitional or turbulent), and on the freestream Mach and Reynolds numbers. The protuberance incipient deflection angle is that where a slight increase in deflection results in an increase in the pressure gradient imposed on the incoming attached boundary layer and induces a separation. Previous studies on two-dimensional compression corner interactions have determined the incipient separation angle for certain freestream conditions (Chapman et al. 1958; Hakkinen et al. 1959; Sterrett and Emery 1960; Needham and Stollery 1966a, 1966b; Elfstrom 1971) as follows:

For laminar flow: $\alpha_i \approx 80 M_\infty^{0.5} \mathrm{Re}_x^{-0.25} \left(\rho_w \mu_w\right)^{0.25} \left(\rho_e \mu_e\right)^{-0.25}$ [Eq. 1]

For turbulent flow: $\alpha_i \approx 11 M_\infty^{0.5}$ [Eq. 2]

4.3 Unseparated interactions

For unseparated interactions ($\alpha < \alpha_i$) the hot spot is located to the side of the protuberance. Ahead of the protuberance the heat flux values are close to the corresponding undisturbed value or slightly lower. The ratio $St_{\max} / St_u$ is plotted for the different cases with the purpose of determining any dependence on the state of the boundary layer (Fig. 18). In the present case, for a fully turbulent boundary layer $St_{\max} / St_u$ is approximately 2.7 whereas for a laminar or transitional boundary layer $St_{\max} / St_u$ is around 6.5. A clearer correlation is observed in a form of Stanton number (Fig. 17) for all the different flow conditions considered (Eq. 3). While this corroborates the inferred state of the boundary layer in Section 2.5, the previous correlations based on the undisturbed boundary layer heat flux are considered misleading given that the state of the boundary layer in the region of amplified heating is believed to be transitional or even fully turbulent. Heat transfer values lower or similar to the corresponding heat transfer in undisturbed flow were measured ahead of the protuberance (Eq. 4). Although the exact location of the hot spot cannot be accurately predicted given its long extent to the side of the protuberance, it is convenient to consider its location from the protuberance leading edge up to a longitudinal distance of about $\mathrm{Re}_{x,k} = 0 - 5\times10^5$, i.e. $x_{k,\max} = 0 - 5\times10^5 \left(\mathrm{Re}_\infty / m\right)^{-1}$ (Eq. 5).

$$St_{\max,side} = 2.7\times10^{-3} \pm 20\% \quad \text{[Eq. 3]}$$

$$St_{\max,ahead} \approx St_u \quad \text{[Eq. 4]}$$

$$x_{k,\max} = 0 - 5\times10^5 \left(\mathrm{Re}_\infty / m\right)^{-1} \text{ to protuberance side} \quad \text{[Eq.5]}$$

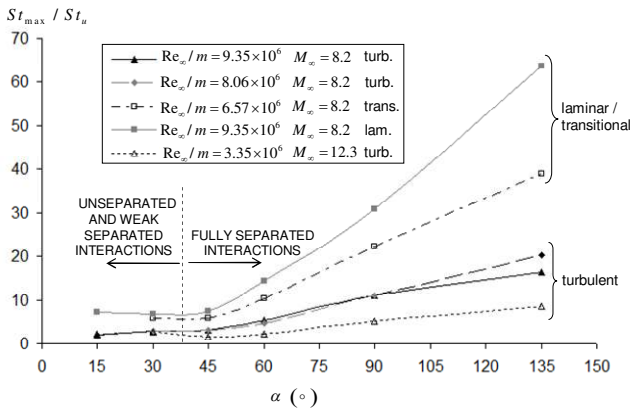

Fig. 18 Maximum heat flux in $St_{\max} / St_u$ for all the different configurations.

4.4 Fully separated interactions

For fully separated cases the hot spot is generally found ahead of the protuberance and its magnitude is independent of the state of the incoming boundary layer. While this could possibly be related to stagnation conditions as also hypothesized by Nestler (1985), no supporting evidence is found with the present dataset neither since the physical mechanisms that induce high heating ahead of protuberances with separated interactions do not directly correlate with the relevant relations considered in the classic stagnation heat transfer theory (Fay and Riddell 1958). Given that the highest heat flux ahead of the α=135° cases is strongly dependent on the location where the separated flow reattaches to the surface and also since there is a clear increase in heat flux as the deflection angle is increased, it seems obvious that the maximum heating is linked to the reattachment of the flow ahead of the protuberance also (Section 4.5). In this way, as the protuberance deflection angle is increased, the deflection that the incoming flow experiences before reattaching to the wall is lower and so its impact energy to the surface is higher. This is analyzed in more detail in Appendix A, where a further assessment of the results is performed. Based on this analysis, Fig. 19 shows a correlation of the present experimental dataset in terms of the dominant parameters: Reynolds number, Mach number and protuberance deflection angle and height. The actual thermal capacity of the flow is already taken into account in the definition of Stanton number. The correlation provided is subject to a total conservative uncertainty of ±25% while also considering the ±10% uncertainty inherent to the measurements. The maximum heat transfer to the side of the protuberance is as shown in Eq. 6. The hot spot will nevertheless be located ahead of the protuberance in most cases following the relation in Eq. 7. In these cases the hot spot will take place as shown in Eq. 8. Only in low-Reynolds low-deflection cases this will be located to the side of the protuberance as in unseparated interactions (Eq. 5).

$$St_{\max,side} = 2.7\times10^{-3} \pm 20\% \quad \text{[Eq. 6]}$$

$$St_{\max,ahead} = 5.2\times10^{-5}\,\mathrm{Re}_h^{0.6}(1-\cos\alpha)M_\infty^{-0.5} \pm 25\% \quad \text{[Eq. 7]}$$

$$x_{k,\max} = 0 - 5\times10^{4}\left(\mathrm{Re}_\infty/m\right)^{-1} \text{ ahead of protuberance [Eq. 8]}$$

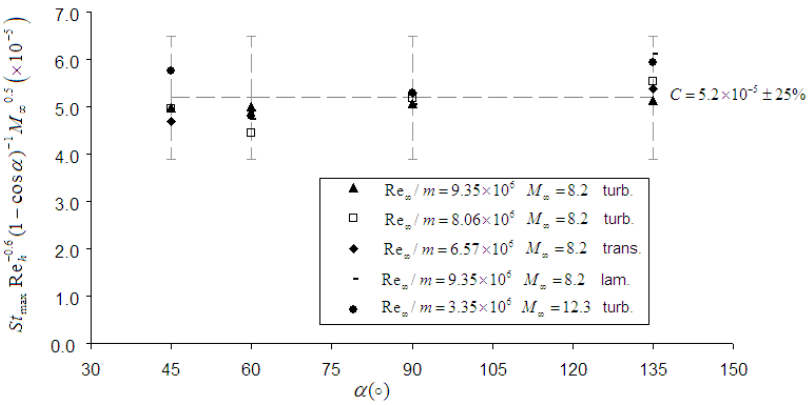

Fig. 19 Correlation of the whole hot-spot experimental dataset showing uncertainty of ±25%.

4.5 Interpretation of the flow field

The following presents interpretation of the experimental results around the protuberance – i.e. heat flux measurements, schlieren videos and oil dot visualizations – assisted by qualitative CFD solutions to help understand the flow structure and characteristics. In the unseparated cases, the flow upstream is clearly undisturbed and close to the centreline of the protuberance this can be considered as quasi-two-dimensional in the y_{cl} direction. The increased heat transfer which occurs to the sides is expected to be caused by corner effects which result in the appearance of a vortex as interpreted in Fig. 20a and similar to the junction horseshoe vortex observed in blunt swept fin interactions (Lakshmanan et al. 1988). The high heating rates appear as a consequence of the flow reattachment to the side of the protuberance. Whereas similar effects on the protuberance side are expected in fully separated interactions, the flow also separates ahead. An example is shown in Fig. 20b based on the case of a α=135° protuberance under turbulent flow, M_∞=8.2 and $Re_\infty/m=9.35\times10^6$. Given high heating ahead of this model is due to the reattachment of the flow and assuming the existence of a large secondary recirculation in comparison to the other separated cases, this may explain the minor upstream movement in the location of the hot spot. The interpretation of fully separated interactions in the vicinity of the protuberances is therefore summarized in the form of two schematic diagrams in Fig. 21.

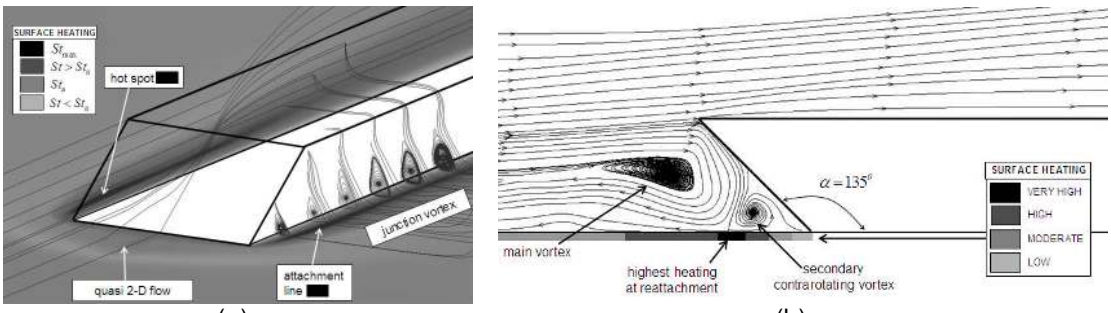

(a) (b)

Fig. 20 Interpretation of the flow field for an unseparated case (a) and ahead of α=135° protuberance (b).

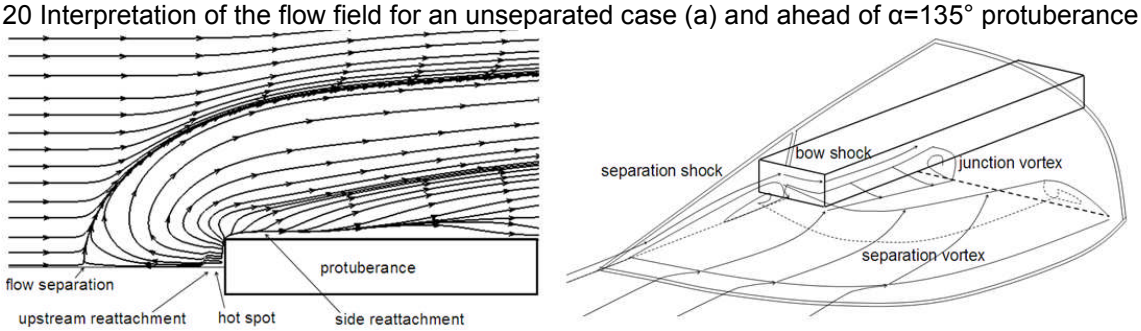

(a) (b)

Fig. 21 Expected flow streamlines illustrating corner effects on fully separated interaction (a) and expected flow field around the protuberance (b).

4.6 Hot spot estimation approach

Based on these findings and on the current semi-empirical correlations a summary for an engineering method for hot-spot estimation is presented in Fig. 22. The initial step is to estimate whether the interaction is unseparated or fully separated based on two-dimensional compression corner experimental data. In this case, high heat transfer regions around the protuberance are indicated and the location and magnitude of the hot spot can be estimated by using the derived semi-empirical correlations. It is particularly the highest heating ahead of the protuberances which can become critical in the design of hypersonic vehicles. More accurate estimations can be obtained in this case referring directly to Fig. 23 for the corresponding angle and Mach number. In this way, the uncertainty introduced by the correlations of deflection angle and Mach number is avoided and final estimates can be obtained with an uncertainty of ±15%. It must be noted that these semi-empirical correlations are based on well-defined forms of protuberances which do not account for other effects such as side sweep or skewness. Besides, all the tests were performed at an initial wall temperature of T_w=295±5 K and therefore the effect of wall temperature is not addressed either. A further discussion on these aspects can be found in Estruch (2009a).

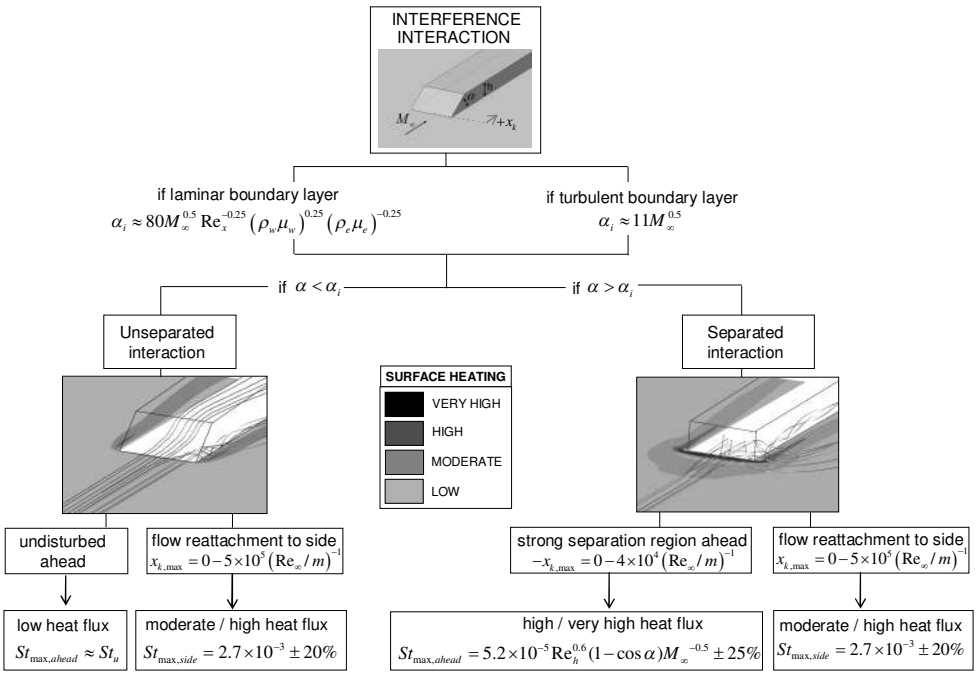

Fig. 22 Engineering approach to predict location and magnitude of highest heating in the vicinity of surface protuberances in hypersonic flow.

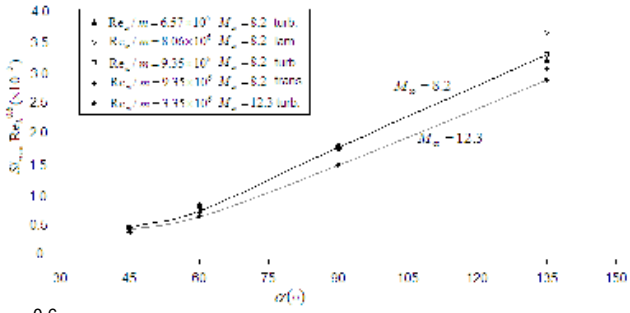

Fig. 23 Correlation of $St_{max}Re_h^{-0.6}$ with protuberance deflection angle α at different freestream Mach numbers.

5. Concluding remarks

An experimental investigation was performed in a hypersonic gun tunnel to study the local heat transfer distributions in the vicinity of a three-dimensional surface protuberance. An experimental dataset of heat flux measurements considering all the main parameters involved in hypersonic interference interactions is presented and a semi-empirical approach is developed to predict the location and magnitude of the hot spot in the vicinity of surface protuberances. The impact of the local interaction on the heating of the vehicle surface is dominated by whether the boundary layer separates ahead of the protuberance or not. The hot spot is found to the side of the protuberance in unseparated interactions. Whereas increased heating is also found to the side of the protuberance in fully separated interactions the hot spot generally takes place ahead of the protuberance and can become significantly high. In this case, the value of the peak heat flux increases with freestream Reynolds number, protuberance height and deflection angle but decreases with Mach number. In both unseparated and fully separated interactions the dependence of maximum heating on the incoming boundary layer state is negligible. This is most likely because the incoming laminar boundary layer becomes transitional or even fully turbulent through the interaction as suggested by the present measurements. This is believed to be directly linked to the 3-dimensionality of the interactions as supported by the analysis of results at all the test conditions. The peak heat flux can be estimated using simple empirical correlations with a total uncertainty of 15% or lower.

Appendix A. Correlation of peak heat flux in fully separated interactions

Buckingham-Pi analysis is used to derive a correlation of the hot spot magnitude in fully separated interactions. This approach is commonly used in the interpretation of experimental data and has previously led to the development of predictive methods for heat transfer in attached flows (Rogers and Mayhew 1980). The main variables responsible for the heat flux need to be determined. It is well established that the main parameters to be considered are viscosity μ, density ρ, thermal conductivity k, specific heat c_p, temperature relative to wall θ, fluid velocity U and a characteristic linear dimension l. As expected from the previous literature (Section 1), the characteristic linear dimension l which has a dominant effect in fully separated interactions is the height of the protuberance (h) whereas the effect of width is known to be negligible. The effect of boundary layer thickness is also considered negligible throughout the present experimental study as shown by the similitude between the peak heating at laminar and turbulent conditions (Section 3.5). Based on a dimensional analysis considering mass, length, time, thermal energy and temperature as the five fundamental units and grouping them in terms of two main non-dimensional groups (Re and Pr) the relation in Eq. 9 is derived, where *a* and *b* are exponents, *C* is a constant and Re_h is Reynolds number based on protuberance height. Since in experimental measurements of this type accurate knowledge of the Prandtl number Pr is generally not feasible, common predictive approaches developed to date consider a constant Prandtl number. For this reason, a common simplification is to assume Pr=1 and Eq. 9 thus reduces to Eq. 10. For more details on the derivation of this relation refer to Rogers and Mayhew (1980). The experimental results obtained at a freestream Mach number of M_∞=8.2 and at Reynolds numbers of Re_∞/m=6.57x10^6, 8.06x10^6 and 9.35x10^6 are used to obtain a correlation of Nu_h with Re_h. The highest heat flux in terms of Nu_h are plotted against Re_h for the α=45°, α=60° and α=90° cases showing a correlation of the measurements with a slope of a=1.6. Since Pr is considered equal to 1, $Nu_h = St_{\max}\,\mathrm{Re}_h$ and a=1.6 are introduced in Eq. 10 to obtain the relation in Eq. 11 (Fig. 24). The recovery factor is also considered to be r=1.

$$Nu_h = C\,\mathrm{Re}_h^a\,\mathrm{Pr}^b \qquad \text{[Eq. 9]}$$

$$Nu_h = C\,\mathrm{Re}_h^a \qquad \text{[Eq. 10]}$$

$$St_{\max}\,\mathrm{Re}_h^{-0.6} = C \qquad \text{[Eq. 11]}$$

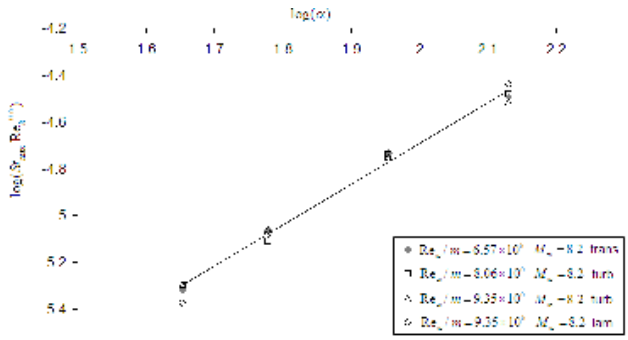

Fig. 24 Correlation of $St_{max}Re_h^{-0.6}$ with protuberance deflection angle α at different freestream Reynolds numbers in logarithmic scale.

The term $St_{\max}\,\mathrm{Re}_h^{-0.6}$ is constant for different Reynolds numbers but it increases with higher deflection angles (Fig. 24). The effect of α is introduced by considering the deflection experienced by the incoming flow before it reattaches to the surface ahead of the protuberance. This is expressed as shown in Eq. 12. Fig. 25 shows the constant trend obtained for the M_∞=8.2 tests at all the different conditions while the same does not apply in the cases where the hot spot takes place to the side of the protuberance - i.e. in unseparated or weak separated interactions. This is because the side heat flux is caused by corner effects (Section 4.5). The effect of Mach number is subsequently investigated through a similar correlation between the M_∞=8.2 and the M_∞=12.3 measurements. Its effect is found to be proportional to the square root of Mach number as shown in Eq. 13. A suitable constant C for the final relation in Eq. 13 is found to be $C = 5.2\times10^{-5}$ as shown in Fig. 19.

$$St_{\max}\,\mathrm{Re}_h^{-0.6}/\left(1-\cos\alpha\right) = C \qquad \text{[Eq. 12]}$$

$$St_{\max}\,\mathrm{Re}_h^{-0.6}\,M^{0.5}/\left(1-\cos\alpha\right) = C \qquad \text{[Eq. 13]}$$

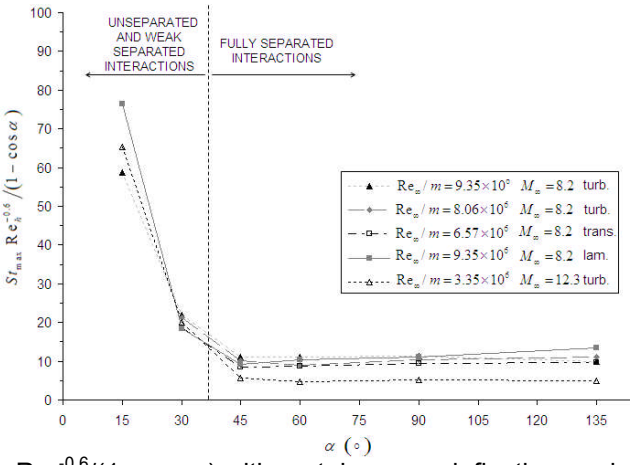

Fig. 25 Correlation of $St_{max}Re_h^{-0.6}/(1 - \cos\alpha)$ with protuberance deflection angle α at different freestream Reynolds numbers.

References

Arrington JP (1968) Heat transfer and pressure distributions due to sinusoidal distortions on a flat plate at Mach 20 in helium. NASA TN D-4907

Bertram MH, Wiggs MM (1963) Effect of surface distortions on the heat transfer on a wing at hypersonic speeds. AIAA J 1(6):1313-1319

Chapman DR, Kuehn DM, Larson KH (1958) Investigation of separated flows in supersonic and subsonic streams with emphasis on the effects of transition. NACA 1356

Coleman HW, Lemmon EC (1973) The prediction of turbulent heat transfer and pressure on a swept leading edge near its intersection with a vehicle. AIAA 73-677

Eckert ERG (1956) Engineering relations for heat transfer and friction in high-velocity laminar and turbulent boundary layer flows over surfaces with constant pressure and temperature. Transactions of the ASME 78(6):1273-1283

Elfstrom GM (1971) Turbulent separation in hypersonic flow. I.C. Aero Report 71-16

Estruch D, Lawson NJ, MacManus DG, Garry KP, Stollery JL (2008) Measurement of shock wave unsteadiness using a high-speed schlieren system and digital image processing. Rev Sci Instrum 79(12):126108-126108-3

Estruch D (2009a) Hypersonic Interference Aerothermodynamics. PhD Thesis, Department of Aerospace Sciences, Cranfield University, Bedford, UK

Estruch D, Lawson NJ, Garry KP (2009b) Application of optical measurement techniques to supersonic and hypersonic aerospace flows. ASCE J Aero Eng 22(4):383-395

Estruch D, Lawson, NJ, MacManus DG, Garry KP, Stollery JL (2009c) Schlieren visualization of high-speed flows using a continuous LED light source. J Vis 12(4):289-290

Estruch D, MacManus DG, Richardson DP, Lawson NJ, Garry KP, Stollery JL (2009d) Experimental study of unsteadiness in supersonic shock-wave/turbulent boundary-layer interactions with separation. Aero J In press

Fay JA, Riddell FR (1958) Theory of Stagnation Point Heat Transfer in Dissociated Air. J Aero Sci 25(2):73-85

Guoliang M, Guiqing J (2004) Comprehensive analysis and estimation system on thermal environment, heat protection and thermal structure of spacecraft. Acta Astron 54(5):347-356

Hakkinen RJ, Greber I, Trilling L (1959) The interaction on an oblique shock wave with a laminar boundary layer. NASA Mem 2-18-59W

Holden MS (1964) Heat transfer in separated flow. PhD Thesis, Imperial College, UK

Hung FT, Clauss JM (1980) Three-dimensional protuberance interference heating in high-speed flow. AIAA-80-0289

Hung F, Patel D (1984) Protuberance Interference Heating in High-Speed Flow. In Proc 19th Thermophysics Conference. AIAA-84-1724

Jones RA (1964) Heat-transfer and pressure investigation of a fin-plate interference model at a Mach number of 6. NASA TN D-2028

Kuehn DM (1959) Experimental investigation of the pressure rise required for the incipient separation of turbulent boundary layers in two-dimensional supersonic flow. NASA Memo 1-21-59W

Lakshmanan B, Tiwari SN, Hussaini MY (1988) Control of supersonic intersection flowfields through filleting and sweep. In proc., 1st National Fluid Dynamics Congress, Cincinanati, Ohio. Part 2:746-759

Meador WE, Smart MK (2005) Reference enthalpy method developed from solutions of the boundary-layer equations. AIAA J 43(1):135-139

Needham DA (1963) Progress report on the Imperial College hypersonic gun tunnel. Report 118

Needham DA, Stollery JL (1966a) Hypersonic studies of incipient separation and separated flows. Aeronautical Res Council paper ARC 27752 Jan 1966

Needham DA, Stollery JL (1966b) Boundary layer separation in hypersonic flow. AIAA 66-455

Nestler DE (1985) The effects of surface discontinuities on convective heat transfer in hypersonic flow. AIAA Paper 85-0971

Neumann RD, Hayes JR (1981) Protuberance heating at high Mach numbers, a critical review and extension of the database. AIAA 81-0420

Olivier H (2009) Thin film gauges and coaxial thermocouples for measuring transient temperatures. SWL, RWTH.

Price EA, Stallings RL (1967) Investigation of turbulent separated flows in the vicinity of fin-type protuberances at supersonic Mach numbers. NASA TN D-3804

Prince SA (1995) Hypersonic turbulent interaction phenomena and control flap effectiveness. MSc Thesis, Cranfield University, Bedford, UK

Rogers GFC, Mayhew YR (1980) Engineering thermodynamics Work and Heat Transfer. Longman Scientific & Technical, John Wiley & Sons, New York

Schultz DL, Jones, TV (1973) Heat-transfer measurements in short-duration hypersonic facilities. AGARD-AG-165

Simmons JM (1995) Measurement techniques in high-enthalpy hypersonic facilities. Exp Therm Fluid Sci 10 (4):454-469

Stainback PC (1969) Effect of unit Reynolds number, nose bluntness, angle of attack, and roughness on transition on a 5° half-angle cone at Mach 8. NASA TN D-4961

Sterret JR, Emery JC (1960) Extension of boundary layer separation criteria to a Mach number of 6.5 by utilizing flat plates with forward facing steps. NASA TN D-618

Sterret JR, Morrissete EL, Whitehead AH Jr, Hicks RM (1967) Transition fixing for hypersonic flow. NASA TN D-4129

Stollery JL, MacManus DG, Estruch D (2008) Hypersonic research and its application to a real vehicle. Seminar presentation.

Vannahme M (1994) Roughness effects on flap control effectiveness at hypersonic speeds. MSc Thesis, Cranfield University, Bedford, UK

Wang SF, Ren ZY, Wang Y (1998) Effects of Mach number on turbulent separation behaviours induced by blunt fin. Exp Fluids 25:347-351

Wang XY, Yuko J, Motil B (2009) Ascent heating thermal analysis on the spacecraft adaptor (SA) fairings and the interface with the crew launch vehicle (CLV). NASA TM-2009-215474

Weinstein LM (1970) Effects of two-dimensional sinusoidal waves on heat transfer and pressure over a flat plate at Mach 8. NASA TN D-5937

White FM (2006) Viscous Fluid Flow, 3rd Edition. McGraw Hill, New York